Mechanical Steering Compensators for High-Performance Motorcycles

Simos Evangelou
e-mail: s.evangelou@imperial.ac.uk

David J. N. Limebeer[1]
e-mail: d.limebeer@imperial.ac.uk

Robin S. Sharp
e-mail: robin.sharp@imperial.ac.uk

Department of Electrical and Electronic Engineering,
Imperial College London,
London SW7 2AZ, UK

Malcolm C. Smith
Department of Engineering,
University of Cambridge,
Cambridge CB2 1PZ, UK
e-mail: mcs@eng.cam.ac.uk

This paper introduces the idea of using mechanical steering compensators to improve the dynamic behavior of high-performance motorcycles. These compensators are seen as possible replacements for a conventional steering damper and comprise networks of springs, dampers, and a less familiar component called the inerter. The inerter was recently introduced to allow the synthesis of arbitrary passive mechanical impedances, and finds a potential application in the present work. The design and synthesis of these compensation systems make use of the analogy between passive electrical and mechanical networks. This analogy is reviewed alongside the links between passivity, positive reality, and network synthesis. Compensator design methods that are based on classical Bode-Nyquist frequency-response ideas are presented. Initial designs are subsequently optimized using a sequential quadratic programing algorithm. This optimization process ensures improved performance over the machine's entire operating regime. The investigation is developed from an analysis of specific mechanical networks to the class of all biquadratic positive real functions. This aspect of the research is directed to answering the question: "What is the best possible system performance achievable using any simple passive mechanical network compensator?" The study makes use of computer simulations, which exploit a state-of-the-art motorcycle model whose parameter set is based on a Suzuki GSX-R1000 sports machine. The results show that, compared to a conventional steering damper, it is possible to obtain significant improvements in the dynamic properties of the primary oscillatory modes, known as "wobble" and "weave."
[DOI: 10.1115/1.2198547]

1 Introduction

The dynamics of motorcycles and their possible modes of instability have been studied for decades. In the case that one or more of these modes is stable, but lightly damped, the potential exists for undesirable responses to uneven road surfaces. Early research on motorcycle dynamics was confined to the relatively simple case of small perturbations from straight running [1–3]. In later work, models were extended to include small perturbations from a steady-state cornering condition [4–9]. It is clear from these studies that under certain operating conditions some of the machine's modes can be lightly damped, or even unstable. It is also clear that the lightly damped modes can be excited by road undulations [10]. Reference [10] refers to several real-life incidents in which resonant-forcing-type phenomena ended unhappily for the rider. In addition to this theoretical work, motorcycle oscillations have been widely studied via measurement programs [11–25].

The main lateral oscillations in two-wheeled vehicles are "wobble" and "weave." In straight running, the weave mode is well damped at moderate speeds, but becomes less so as the machine's forward speed increases. The natural frequency rises from zero at very low speed to somewhere in the range 2–4 Hz, depending on the mass and size of the machine, the lower frequencies corresponding to heavier motorcycles. The only properly documented wobble oscillations involve moderate speeds, although there are many anecdotal accounts of wobble at high speeds [26]. Theoretical results indicate that the torsional stiffness of the motorcycle frame at the steering head determines whether a machine will be prone to wobbling at medium speeds (compliant frame) or at high speeds (stiff frame) [27,28]. The frequency of the wobble mode is relatively independent of speed and is governed primarily by the mechanical trail, the front tire cornering stiffness and the front frame steer inertia. The wobble mode's frequency is normally in the range 6–9 Hz. Stiff framed machines, being prone to wobbling at high speed, often depend on a steering damper for satisfactory wobble-mode damping. Normally, however, a steering damper will destabilize the high-speed weave mode. In cornering, the above lateral modes and the in-plane modes associated with tire deflections and suspension motions become coupled, as was first shown in any detail by Koenen [4]. The motorcycle becomes prone to resonant forcing via regular road undulations when the displacement forcing they produce is tuned to lightly damped modal frequencies of the machine. Moderate roll angles are likely to represent the worst-case conditions [10].

The free steering system of a single-track vehicle is essential to its stability and control behavior [7]. It enables the machine to self-steer, to some extent, and it allows the rider to operate in free control, or provide a steering torque input for directional control purposes. Modifications to the machine in the steering head region that impact the steering geometry, the frame compliance, and the steering damping are particularly influential. The question naturally arises: "are there better ways of influencing the self-steering action than through the use of conventional steering dampers?" One approach to the problem posed by this question is described in [29], where an adaptive damper is considered as a means of alleviating a wobble-related phenomenon known as "kickback." Kickback is a sharp change is steering angle that results from high-speed running over rough surfaces. An interesting feature of this work is the preservation of the low-speed light handling of the

[1]Author to whom correspondence should be addressed.

Contributed by the Applied Mechanics Division of ASME for publication in the JOURNAL OF APPLIED MECHANICS. Manuscript received November 4, 2004; final manuscript received March 1, 2006. Review conducted by O. M. O'Reilly. Discussion on the paper should be addressed to the Editor, Prof. Robert M. McMeeking, Journal of Applied Mechanics, Department of Mechanical and Environmental Engineering, University of California – Santa Barbara, Santa Barbara, CA 93106-5070, and will be accepted until four months after final publication of the paper itself in the ASME JOURNAL OF APPLIED MECHANICS.

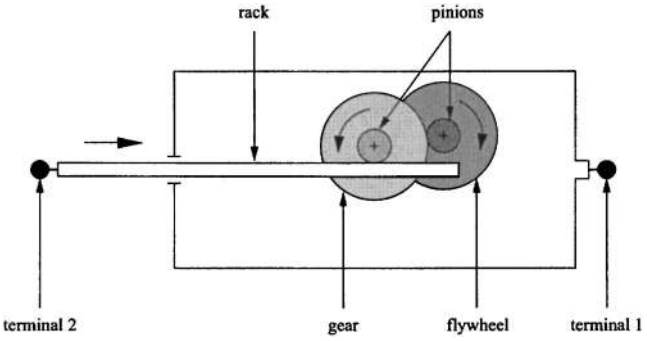

Fig. 1 Schematic of an inerter embodiment

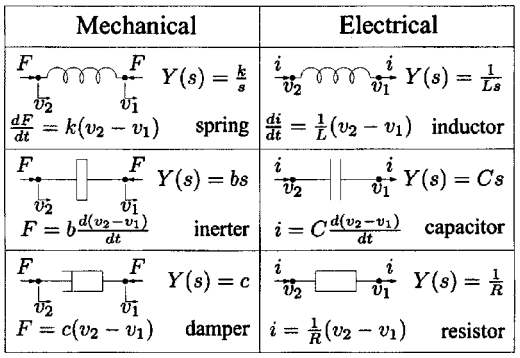

Fig. 2 Circuit symbols and electromechanical correspondences with defining equations and admittances $Y(s)$

machine. The simultaneous suppression of kickback and low-speed maneuverability preservation led to the speed- and acceleration-based adaptive damping scheme described. The purpose of the present paper is to introduce a phase-compensation-based approach to the design question posed earlier in the paragraph. This compensation is achieved using passive mechanical networks consisting of springs, dampers, and inerters.

The paper is organized as follows. Section 2 reviews the nature and properties of the inerter, which is still a relatively unfamiliar mechanical component. Some of the basic elements of electrical-mechanical circuit analogies, passive network synthesis, and positive reality are briefly reviewed. In Sec. 3, the background to the motorcycle model is described. Some of the important characteristics of the reference motorcycle-rider system are described in Sec. 4. Frequency-response-based design procedures for simple mechanical networks are given in Sec. 5. A procedure for optimizing the parameter values of arbitrary passive steering compensators is given in Sec. 6. Both time- and frequency-domain approaches to parameter optimization are studied. The influence and performance of the base motorcycle fitted with various steering compensators are evaluated in Sec. 7. Conclusions are drawn in Sec. 8.

2 Network Synthesis

2.1 The Inerter. A two-terminal mechanical element called the inerter was introduced in [30] with the property that the (equal and opposite) force applied at the terminals is proportional to the relative acceleration between them. The inerter obeys the force-velocity law $F=b(\dot{v}_1-\dot{v}_2)$, where the constant of proportionality b is called the inertance and has the units of kilograms. In order to be practically useful, the device should have a small mass (relative to b) and its inertance should be adjustable independently of the mass. Also, the device should function properly in any spatial orientation, it should support adequate linear travel and should have reasonable overall dimensions. One way in which such a device can be made with the required properties is illustrated in Fig. 1. It comprises a plunger that is constrained to translate relative to a housing, which then drives a flywheel via a rack and pinion, and gears. For such devices, the value of the inertance b is easy to compute in terms of the various gear ratios and the flywheel's moment of inertia [30]. In general, if the device gives rise to a flywheel rotation of α radians per meter of relative displacement between the terminals, then the inertance of the device is given by $b=J\alpha^2$ where J is the flywheel's moment of inertia. Various embodiments of inerters are described in [31], and several prototype devices have been built and tested in the Engineering Department at Cambridge University.

A rotational version of the inerter can also be defined, namely, a device where the (equal and opposite) torque applied at each terminal (which can be separately rotated) is proportional to the relative angular acceleration between the terminals. The inertance of such a device is measured in kilogram meter squared. Embodiments in pure rotational form can be devised, by making use of epicyclic gears, for example [31]. For an ideal device of this type in which there is a gear ratio of n between rotations of the terminals and rotations of a flywheel with moment of inertia J, the inertance is given by Jn^2.

2.2 Passive Circuit Synthesis. One of the principal motivations for the introduction of the inerter in [30] was the synthesis of passive mechanical networks. It was pointed out that the standard form of the electrical-mechanical analogy (in which the spring, mass, and damper are analogous to the inductor, capacitor, and resistor) was restrictive for this purpose, because the mass element effectively has one terminal connected to ground. In order that the full power of electrical circuit synthesis theory be translated over to mechanical networks, it is necessary to replace the mass element by a genuine two-terminal element—the inerter. Figure 2 shows the new table of element correspondences in the force-current analogy where force and current are the "through" variables, and velocity and voltage are the "across" variables. The admittance $Y(s)$ is the ratio of through to across quantities, where s is the standard Laplace transform variable. For mechanical networks in rotational form, the through and across variables are torque and angular velocity, respectively. For further background on network analogies, the reader is referred to [32].

The theory of passive circuits has been widely studied in the electrical engineering literature [33,34]. The concept of passivity can be translated over directly to mechanical networks as follows. Suppose that (F,v) represents the force-velocity pair associated with a two-terminal mechanical network, then passivity requires

$$E(T) = \int_{-\infty}^{T} F(t)v(t)dt \geq 0 \tag{1}$$

for all admissible force-velocity pairs. The integral in (1) represents the energy supplied to the mechanical network. An important class of (rational) functions that relate to passivity are the positive real functions.

The following theorem is taken from [33,34]; see, for example, page 96 of [34].

THEOREM 1. *Let $Z(s)$ be the real rational immittance*[2] *function of a linear time-invariant two-terminal network. Then the network is passive if and only if*

1. *$Z(s)$ has no pole in $Re(s)>0$;*
2. *$Re[Z(j\omega)]\geq 0$ for all real ω, in the case that $j\omega$ is not a pole of $Z(s)$;*
3. *If $j\omega_0$ is a pole of $Z(s)$, it is at most a simple pole, and the residue $Z_{j\omega_0}=\lim_{s\to j\omega_0}(s-j\omega_0)Z(s)$ in the case that ω_0 is fi-*

[2]The immittance function of a network refers to either its impedance or admittance function.

nite, and $Z_\infty = \lim_{s\to\infty} Z(s)/s$ *in the case that* $Z(s)$ *has a pole at infinity, is non-negative.*

Real rational functions satisfying the above conditions are termed *positive real*. If $Z(s)$ is positive real, there exists a two-terminal mechanical network whose impedance equals $Z(s)$, which consists of a finite interconnection of springs, dampers, and inerters [30].

The work presented here will make use of a characterization of biquadratic positive-real functions. This result is often quoted without proof in the electrical circuit literature (e.g., [35], problem 4-18, and [36]). A full proof of necessity and sufficiency is provided in the Appendix.

THEOREM 2. *Consider the biquadratic real rational function*

$$Z(s) = \frac{a_2 s^2 + a_1 s + a_0}{d_2 s^2 + d_1 s + d_0}$$

where $a_2, a_1, a_0, d_2, d_1, d_0$ *are all non-negative and at least one of* d_0, d_1, d_2 *is positive. Then* $Z(s)$ *is positive real if and only if*

$$a_1 d_1 \geq (\sqrt{a_0 d_2} - \sqrt{d_0 a_2})^2$$

2.3 Applications. Various inerter-based mechanical network applications are outlined in [30]. These include (i) the simulation of a mass element without the need for a large mass, (ii) an alternative solution to vibration absorption problems, but without the requirement to mount additional mass-spring elements on the main body, and (iii) a new element in road vehicle suspension systems. In traditional four-wheeled vehicle suspension problems, the suspension system makes use of springs and dampers to connect together the sprung and unsprung masses. The limitations of such an approach are analogous to attempts to synthesize a driving-point impedance via resistors and inductors alone—it is possible to achieve a far broader class of passive circuits if capacitors are also available. The inerter allows a similar broadening for mechanical impedances. The possible benefits of using inerters in passive vehicle suspensions have been explored in [37]. In the present paper, the application of the inerter to motorcycles is considered only in respect of the steering system.

3 Motorcycle Model

The dynamics of motorcycles and the model used to represent them involve three translational and three rotational freedoms of the main frame, a steering freedom associated with the rotation of the front frame relative to the main frame, and the influences of spinning road wheels. The mathematical model employed here also accommodates front and rear suspension freedoms, frame twisting, aerodynamic forces and moments, and the rolling of the rider's upper body relative to the main frame. The forces and moments associated with the tires are modeled using "magic formulas" whose parameters have been optimized to fit measured rig data [38–41]. The tire models used here have been qualified against the contemporary measured data given in [6,42]; these details can be found in [43]. A motorcycle model incorporating all of the above features is described in detail elsewhere; it begins in [5] and is extended in [8,9]. The simulation model is written in LISP and makes use of the multibody modeling code AUTOSIM [44]. The source code can be obtained from the web site http://www.imperial.ac.uk/controlandpower/motorcycles/. The motorcycle's physical geometry is shown in Fig. 3, in which the masses are represented by circles, each with diameter proportional to the mass involved. The AUTOSIM™ [44] model can be configured as either "linear" or "nonlinear." In the latter case, a simulation program results in which the describing equations of motion are solved using numerical integration. The simulation program is used to find equilibrium trim states, which typically involve a fixed target lean angle and a fixed target speed. In the linear configuration, the system is symbolically linearized for small perturbations about a general trim condition. A MATLAB "M" file that sets up the linear model in state-space form is generated automatically. The parameters used in the model derive from laboratory experiments conducted on a contemporary commercially available sports machine [9], the Suzuki GSX-R1000. The effects of a steering damper or a more general steering compensator can be incorporated via the differential equations that describe it. For the particular purposes of the study presented here, the steering compensation system is separated from the rest of the model in the generalized regulator feedback structure [45] shown in Fig. 4. See [46] for a similar use of a control systems paradigm applied to car suspensions. Although this figure shows a frequency-domain model of the linearized system, it is equally applicable to nonlinear time-domain studies. The steering compensator appears as $K(s)$. If $P(s)$ is partitioned as

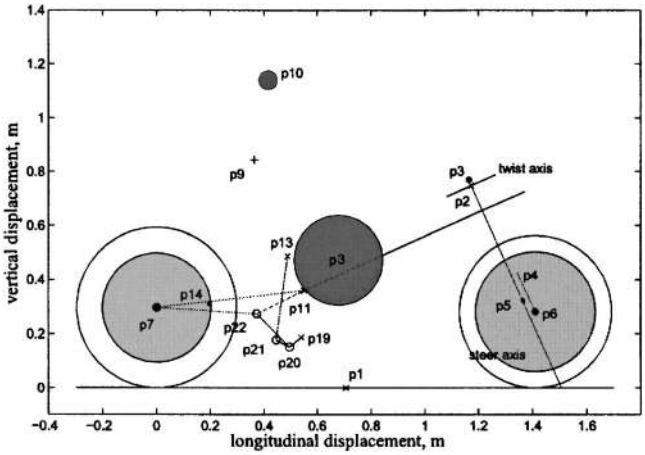

Fig. 3 Scaled diagrammatic motorcycle and rider in side view. The motorcycle-and-rider model shows the machine layout with each of the masses depicted as a proportionately scaled shaded circle.

$$P(s) = \begin{bmatrix} P_{11}(s) & P_{12}(s) \\ P_{21}(s) & P_{22}(s) \end{bmatrix}$$

then the generalized regulator configuration is defined by

$$\begin{bmatrix} \delta(s) \\ s\delta(s) \end{bmatrix} = \begin{bmatrix} P_{11}(s) & P_{12}(s) \\ P_{21}(s) & P_{22}(s) \end{bmatrix} \begin{bmatrix} d(s) \\ T_s(s) \end{bmatrix}$$

and

$$T_s(s) = K(s) s\delta(s)$$

which gives

$$\delta(s) = [I - sP_{12}(s)K(s)]^{-1} P_{11}(s) d(s)$$

since $P_{21}(s) = sP_{11}(s)$ and $P_{22}(s) = sP_{12}(s)$. Repeated reference will be made to Nyquist diagrams and the Nyquist criterion (for an elementary account, see [47], Sec. 9.3) of the open-loop system

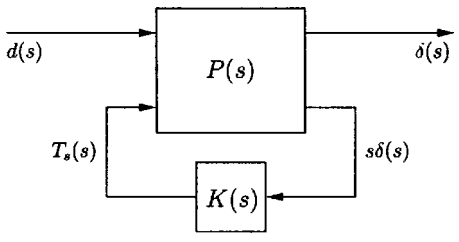

Fig. 4 Feedback arrangement in which $P(s)$ is the linearized motorcycle model and $K(s)$ is the steering compensator. The signal $d(s)$ represents vertical road displacement disturbances, $T_s(s)$ is the steering torque and $\delta(s)$ is the steering angle.

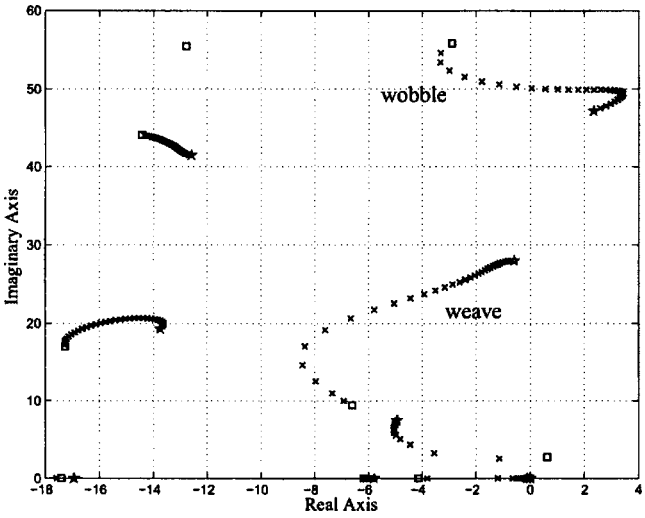

Fig. 5 Root-locus plot for the straight-running motorcycle with speed the varied parameter. No steering damper is fitted. The speed is increased from 5 m/s (□) to 85 m/s (⋆).

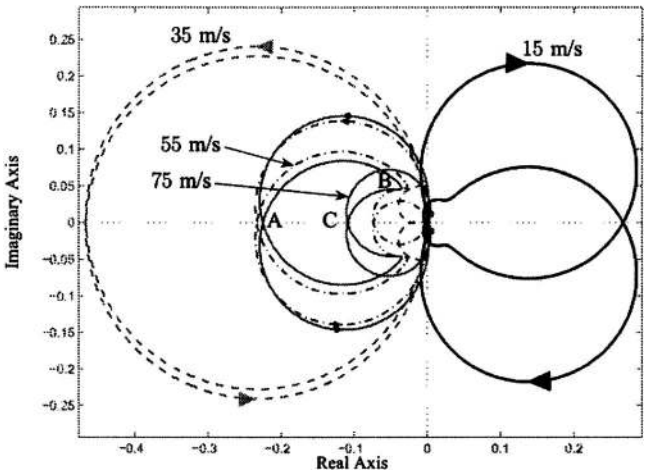

Fig. 7 Straight-running Nyquist diagrams for the open-loop motorcycle model for four different values of forward speed. On the 75 m/s locus, the frequency at A is 47.6 rad/s, at B it is 33.8 rad/s, and at C it reduces to 28.4 rad/s.

$sK(s)P_{12}(s)$, in which $P_{12}(s)$ maps the steering torque $T_s(s)$ into the steering angle $\delta(s)$.

As has been explained elsewhere [5,8,10], speed and steering torque controllers are used in the nonlinear model to establish the steady-state equilibrium state. The reader should understand that these controllers are not included in any of the linearized models or any of the results presented here.

4 Characteristics of the Standard Machine

The important oscillatory modes associated with "wobble" and "weave" are illustrated in the root-locus diagrams of Figs. 5 and 6. Figure 5 corresponds to the straight-running machine with the steering damper removed. It can be seen from this diagram that the wobble-mode frequency varies between 47 and 57 rad/s, while the weave mode's resonant frequency varies between 10 and 28 rad/s. It is clear that the damping of the wobble mode decreases with increased speed, and the mode becomes unstable at ~25 m/s. Figure 6 shows root-loci for the machine with the nominal steering damper fitted for four values of lean angle.

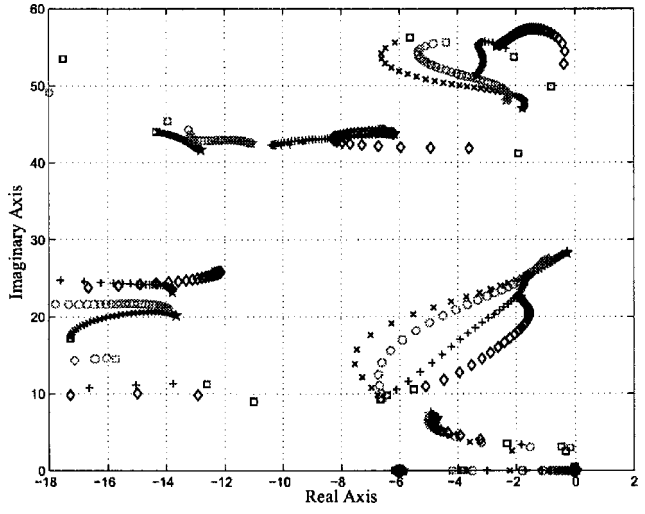

Fig. 6 Root-locus plots for: Straight running (×), 15 deg (∘), 30 deg (+), and 45 deg (◇) of roll angle with speed the varied parameter. The nominal steering damper is fitted. The speed is increased from 7 m/s (□) to 75 m/s (⋆).

Figures 5 and 6 show that the steering damper stabilizes the wobble mode. It also reduces the damping of the weave mode. Figure 6 also shows that increased values of roll angle tend to increase the high-speed weave-mode damping. Since the coupling between the in-plane and out-of-plane dynamics increases with roll angle, one expects the weave mode's vulnerability to road displacement forcing to maximize at an intermediate value (of ~15 deg [10]). It can also be seen from Fig. 6 that for roll angles of up to 30 deg, the high-speed wobble-mode damping increases with roll angle. Further increases in roll angle then destabilize this mode. At low speeds, the wobble-mode damping decreases monotonically with roll angle, and the vulnerability of this mode is worst at low speed and high roll angles.

The open-loop linearized motorcycle model can also be used to generate the Nyquist diagrams shown in Fig. 7. Frequency response plots for straight running at four different values of forward speed are considered. In the case of a steering damper as the compensator in the feedback loop of Fig. 4, $K(s)$ becomes a constant, K, say. It follows from the well-known Nyquist criterion [47] that closed-loop stability requires N anticlockwise encirclements of the $-1/K$ point, where N is the number of unstable poles of the open-loop system and K is the value of the steering damping. At low speeds, both the wobble and weave modes are stable (see Fig. 5), and therefore, no encirclements of the $-1/K$ point are required for the 15 m/s case as shown in Fig. 7. At 35 m/s, the wobble mode of the nominal motorcycle, without its steering damper, becomes unstable as the corresponding complex conjugate pair of poles crosses the imaginary axis into the right-half plane. Under these operating conditions, two counterclockwise encirclements of the $-1/K$ point are therefore required. For higher speeds, two counterclockwise encirclements of the $-1/K$ point are also required, but the range of damper values that will achieve this reduces. Indeed, if the steering damping value is too low, the wobble mode becomes unstable and if it is set too high, the weave mode becomes unstable. In order to appreciate this aspect of the motorcycle's behavior, the reader is referred to the 75 m/s locus in Fig. 7. If the steering damping is set at a low value such that the $-1/K$ point is located at A, the system is on the stability boundary and will oscillate at 47.6 rad/s, which is the wobble-mode frequency. If the steering damper is now increased, two counterclockwise encirclement of the $-1/K$ point result and the machine will be stable. If the steering damper is increased further so that the $-1/K$ point is coincident with the point C, the machine will oscillate at 28.4 rad/s, indicating that the weave mode is on the stability boundary. Any further increases in the steering damper

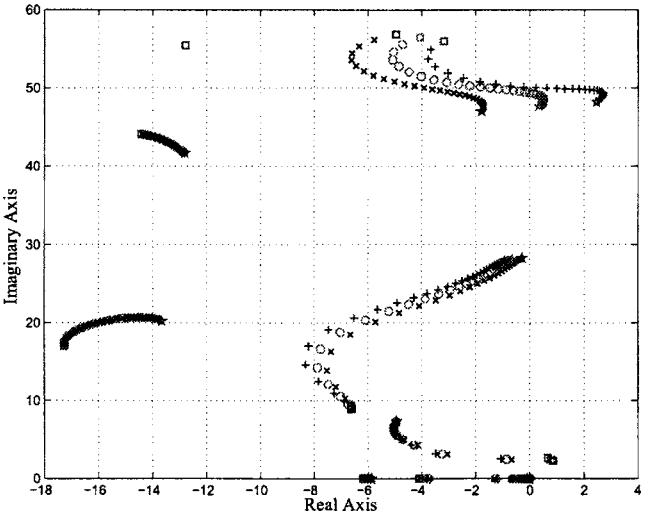

Fig. 8 Straight-running root-loci with speed the varied parameter. The speed is increased from 5 m/s (□) to 75 m/s (⋆). The × locus represents the nominal machine damping value, ∘ refers to a steering damping decrease of 3 Nms/rad, and + to a steering damping reduction of 6 Nms/rad.

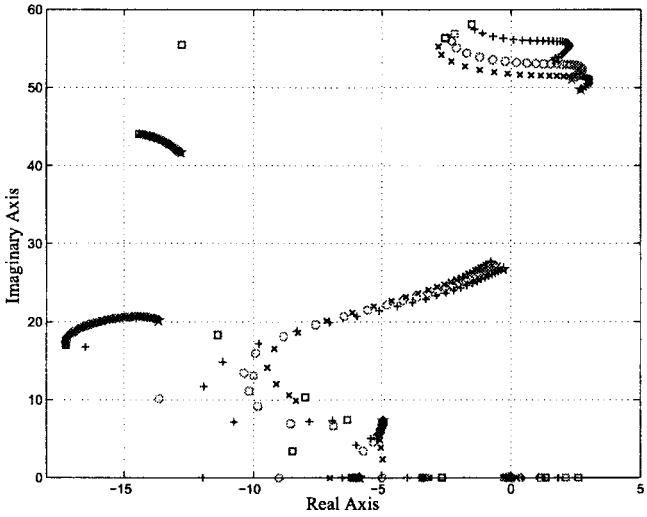

Fig. 9 Straight-running root-loci with speed the varied parameter. The speed is increased from 5 m/s (□) to 75 m/s (⋆). The × locus represents the nominal machine without a steering damper, but fitted instead with a torsional spring of 100 Nm/rad, ∘ represents a spring of 200 Nm/rad, and + corresponds to a spring of 400 Nm/rad.

will render the machine unstable because the $-1/K$ point is not encircled at all. The nominal steering damper value is 6.944 Nms/rad thereby locating the $-1/K$ point at −0.144, which is approximately midway between points A and C in Fig. 7.

5 Frequency Response Design

5.1 Preliminary Observations. In order to develop design methodologies for passive steering compensators, the influences of the damper, the spring, and the inerter, as isolated components, are studied briefly. This will be done by investigating their effect on the wobble- and weave-mode damping and stability. It can be seen from Fig. 8 that the introduction of a steering damper improves the damping of the wobble mode. When the steering damper coefficient value is reduced, the wobble mode becomes unstable at high speed, while the high-speed weave-mode damping increases. The damper has almost no effect on the natural frequency of either of these modes.

Figure 9 shows the effect of a simple torsional spring on the machine's modal damping. As the torsional stiffness is increased, the wobble-mode natural frequency increases and the mode becomes less unstable. At intermediate and high speeds, the wobble mode is unstable for all spring stiffness values. The spring has almost no effect on the weave mode, particularly at high speed, where the weave-mode damping is low.

Figure 10 illustrates the effect on the machine's modal damping characteristics of introducing an inerter. It may be observed that the wobble mode natural frequency reduces as the value of inertance is increased. This is to be expected, since the wobble mode chiefly involves rotation of the front frame assembly; thus, the change is similar to increasing its moment of inertia. It also makes the wobble mode more unstable and increases the damping of the weave mode. When comparing Figs. 8 and 10, one is drawn to the idea that an effective steering compensator should "look like" an inerter at low frequencies in order to improve the damping of the weave mode, while taking on the mantle of a damper at higher frequencies in order to stabilize the wobble mode. This can be interpreted as a form of lead compensation [47].

5.2 Candidate Networks. Beyond the three simple one-element networks considered in Sec. 5.1, the next simplest possibilities are those containing two components. It is easy to show that the three possible pairwise parallel networks have admittance functions: $c+k/s$, $c+sb$, and $(s^2+k/b)/(s/b)$; b, c, and k are used to denote inertance, damping coefficient, and spring stiffness, respectively. The first of these networks takes the form of a proportional-plus-integral compensator, the second is a proportional-plus-derivative compensator, and the third is a notch filter with blocking frequency k/b. Only the second provides the desirable phase-advance property identified in Sec. 5.1 for weave-mode stability, but this occurs above rather than below a specified frequency. The third network suggests the interesting idea of a compensator that is "tuned" to block the high-speed weave-mode range of frequencies. However, this network does not provide damper-like characteristics over the wobble range of frequencies.

The three possible pairwise series networks have transfer functions: $ck/(sc+k)$, $scb/(sb+c)$, and $sk/(s^2+k/b)$. The first of these networks is a lag compensator, the second is a lead compensator,

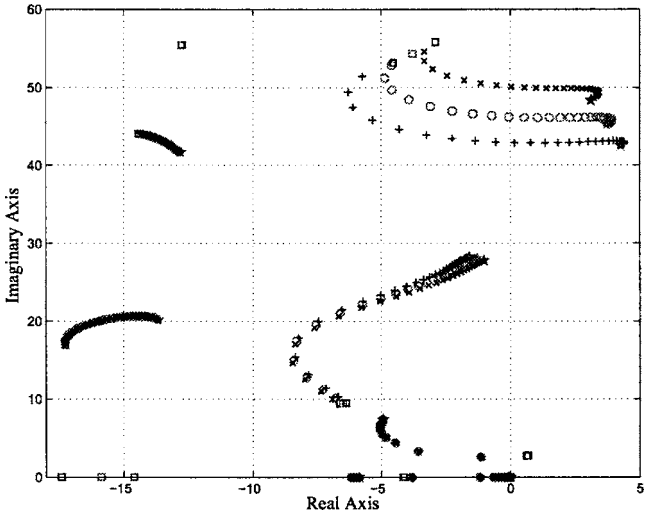

Fig. 10 Straight-running root-loci with speed the varied parameter; the speed is increased from 5 m/s (□) to 75 m/s (⋆). The × locus represents the nominal machine without a steering damper, ∘ represents the effect of an inertance of 0.1 kgm^2, and + the influence of an inertance of 0.2 kgm^2.

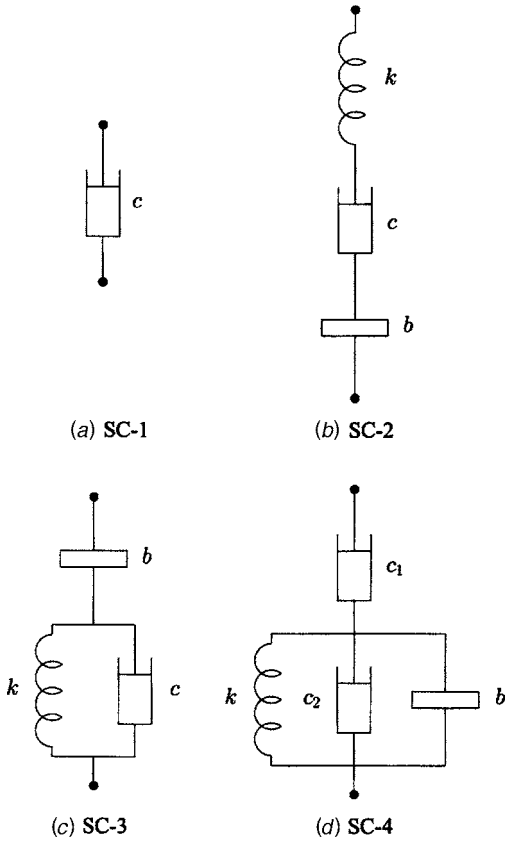

Fig. 11 Simple steering compensation networks

while the third has a resonant frequency at $\omega_0=\sqrt{k/b}$. Among these, the second is the most promising because it has inerter-like (phase-lead) characteristics at low frequencies and damper-like behavior at higher ones. The preliminary observations in Sec. 5.1 have identified such a frequency characteristic as being potentially suitable.

Extending the above type of reasoning to networks with three or four components allows a number of networks to be selected as potentially promising candidate steering compensators for further study. These are shown in Fig. 11. Alongside the conventional damper (steering compensator) SC-1, is the compensation network comprising a damper, spring, and inerter in series (SC-2). This network is a generalization of the two-component device $scb/(sb+c)$ identified above. The important added generality afforded by SC-2 facilitates a rapid phase change in the neighborhood of the resonant frequency $\omega_n=\sqrt{k/b}$. As with the series connected damper-inerter combination, SC-2 has the characteristics of an inerter at low frequencies. The SC-2 network is damper-like in the neighborhood of ω_n and spring-like at high frequencies. In our application, ω_n will be tuned to the wobble-mode frequency so as to introduce damping there.

Network SC-3 has lead networklike properties, and the spring allows fast phase changes through the transition region. Since a damper improves the wobble-mode damping, while having a deleterious effect on the weave-mode characteristics, benefit might be derived from a network which "notches out" the effect of a damper over the weave-mode frequency band. A mechanical network with notch filter characteristics is shown as SC-4 in Fig. 11.

The admittance functions for the networks in Fig. 11 are as follows:

$$Y_1(s)=c$$

$$Y_2(s)=k\frac{s}{s^2+sk/c+k/b}$$

$$Y_3(s)=c\frac{s(s+k/c)}{s^2+sc/b+k/b}$$

$$Y_4(s)=c_1\frac{s^2+sc_2/b+k/b}{s^2+s(c_1+c_2)/b+k/b}$$

It may be observed that the above admittances are at most second-order rational functions and are special cases of the positive-real biquadratic functions of Theorem 2. This class may still be synthesized using springs, dampers, and inerters (although the number of elements may be larger than that required in the networks shown in Fig. 11). It is appropriate to add the idealized case

$$Y_5(s)=\frac{a_2s^2+a_1s+a_0}{d_2s^2+d_1s+d_0}$$

as a further candidate admittance, with the parameters a_0, a_1, a_2, d_0, d_1, d_2 constrained by the conditions of Theorem 2. Although we will not show a circuit realization of $Y_5(s)$, we will refer to this configuration as SC-5.

It is possible to re-parameterize each of the networks SC-2, SC-3, SC-4, and SC-5 in terms of undamped natural frequencies and damping ratios. The admittance function for the network SC-2 may be reparametrized as

$$Y_2(s)=k\frac{s}{s^2+2\zeta\omega_ns+\omega_n^2}$$

in which

$$\omega_n=\sqrt{k/b},\quad \zeta=\frac{\sqrt{bk}}{2c} \tag{2}$$

In the case of SC-3,

$$Y_3(s)=c\frac{s\left(s+\dfrac{\omega_n}{2\zeta}\right)}{s^2+2\zeta\omega_ns+\omega_n^2}$$

in which $\omega_n=\sqrt{k/b}$ and $\zeta=c/(2\sqrt{kb})$.

Similarly,

$$Y_4(s)=c_1\frac{s^2+2\zeta_1\omega_ns+\omega_n^2}{s^2+2\zeta_2\omega_ns+\omega_n^2}$$

in which $\omega_n=\sqrt{k/b}$, $\zeta_1=c_2/(2\sqrt{bk})$ and $\zeta_2=(c_1+c_2)/(2\sqrt{bk})$, and so $\zeta_1<\zeta_2$ is enforced by this network.

In the case of the positive real biquadratic compensator, with a_0, a_2, d_0, $d_2>0$, one obtains

$$Y_5(s)=k\frac{s^2+2\zeta_1\omega_1s+\omega_1^2}{s^2+2\zeta_2\omega_2s+\omega_2^2}$$

in which $k=a_2/d_2$, $\omega_1=\sqrt{a_0/a_2}$, $\omega_2=\sqrt{d_0/d_2}$, $\zeta_1=a_1/(2\sqrt{a_0a_2})$, and $\zeta_2=d_1/(2\sqrt{d_0d_2})$. Then in essence, positive reality comes from satisfaction of the inequality

$$\zeta_1\zeta_2\geqslant\frac{(\omega_1-\omega_2)^2}{4\omega_1\omega_2} \tag{3}$$

As compared to the network SC-4, one is allowed two independent resonant frequencies (rather than one) and the damping ratios need to satisfy the less restrictive constraint (3) instead of $\zeta_2>\zeta_1$.

In the studies which follow, the steering compensator admittance $K(s)$ will be set equal to each of the admittances $Y_1(s),\ldots,Y_5(s)$. For $Y_1(s),\ldots,Y_4(s)$ the parameter values will be

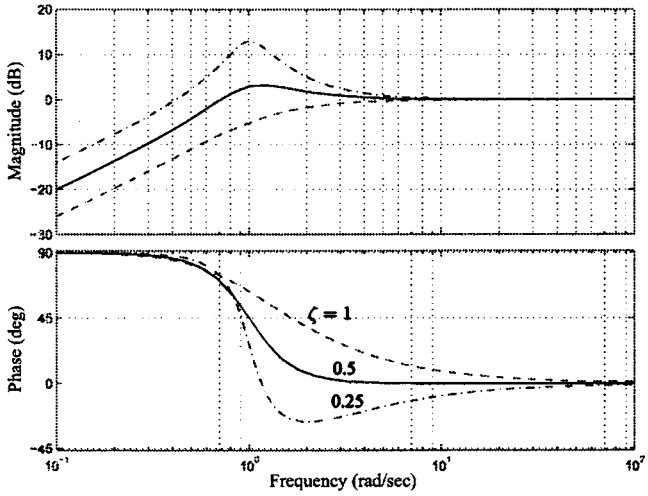

Fig. 12 Normalized frequency responses for SC-3 with unity gain and resonant frequency $\omega_n=1$ for three values of damping ratio ζ

required to be nonnegative, while for $Y_5(s)$ the passivity constraint of Theorem 2 will be imposed; additional networks are considered in the report [48].

5.3 Lead Network Design. The frequency-response characteristics of the compensator SC-3 in Fig. 11 are illustrated in Fig. 12, which has been normalized to $\omega_n=1$. As one would expect, the resonant peak becomes more and more pronounced as the value of ζ is reduced. At the same time, one observes an increasingly rapid phase transition in the neighborhood of ω_n and a smaller value of $\phi_n=\arctan(2\zeta)$, which is the network's phase shift at $s=j\omega_n$.

We now turn to the development of design guidelines for the SC-3 network. A careful examination of the 75 m/s Nyquist plot in Fig. 7 reveals that, for this high-speed straight-running condition, it is advantageous for the steering compensator to introduce phase lead up to the cusp frequency at point B (33.8 rad/s) and proportional gain thereafter; we therefore set $\omega_n=33.8$.

This observation is faithful to the notion that weave requires derivative action, whereas wobble requires proportional compensation. It was established by trial that a damping ratio of $\zeta=0.5$ was suitable. The influence of this unity-gain compensator is illustrated in Fig. 13. As desired, the derivative action has moved the negative-axis crossing point associated with weave-mode instability toward the origin and the crossing point linked to wobble to the left of the diagram. This "opens up" the interval over which two counterclockwise encirclements of the $-1/K$ point can be achieved. In order to maximize the radius of a circle centered at -1, and which can be encircled twice by the Nyquist diagram, the damper coefficient was chosen to be $c=1/0.1741=5.744$. This places the -1 point at the midpoint between the two negative real-axis crossing points. Given these values for c, ζ, and ω_n, the b and k parameters can be found via back substitution using

$$b=\frac{c}{2\zeta\omega_n}$$

$$k=\frac{c\omega_n}{2\zeta}$$

This gives the network parameter values listed in Table 1, and the root-locus plot that results with this mechanical network is shown in Fig. 14. Although the design was based on a single high-speed straight-running linearized model, it is evident that, in comparison with the nominal machine behavior given in Fig. 6, substantial improvements in the damping of the weave mode, under all operating conditions, have been achieved. Greatly improved wobble-mode damping has also been obtained. The improvement in the high-roll-angle (45 deg) case is worthy of particular note.

Table 1 Parameters for network SC-3 given in Fig. 11

c	b	k
5.744	0.1699	194.14

5.4 Notch Filter Design. The frequency-response characteristics of the notch filter network SC-4 in Fig. 11 are illustrated in Fig. 15, in which the depth of the notch is set via ζ_1. Trial and error design studies suggested that the notch frequency should be set below the weave-mode crossing frequency (28.4 rad/s) at point C in Fig. 7 in order that phase lead be introduced above the chosen ω_n value. The following were found to be suitable: ζ_1

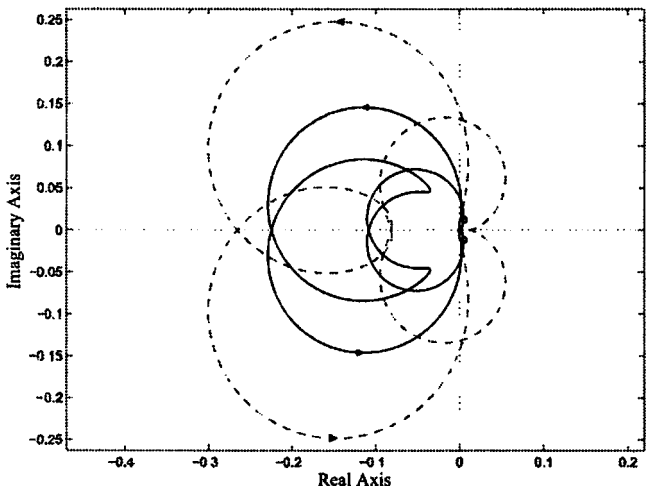

Fig. 13 Nyquist diagram for the straight-running open-loop motorcycle at a forward speed of 75 m/s. The solid line represents the nominal machine with a unity-gain steering damper and the dashed line the compensated system using the SC-3 network given in Fig. 11 ($\omega_n=33.8$, $\zeta=0.5$, $c=1$).

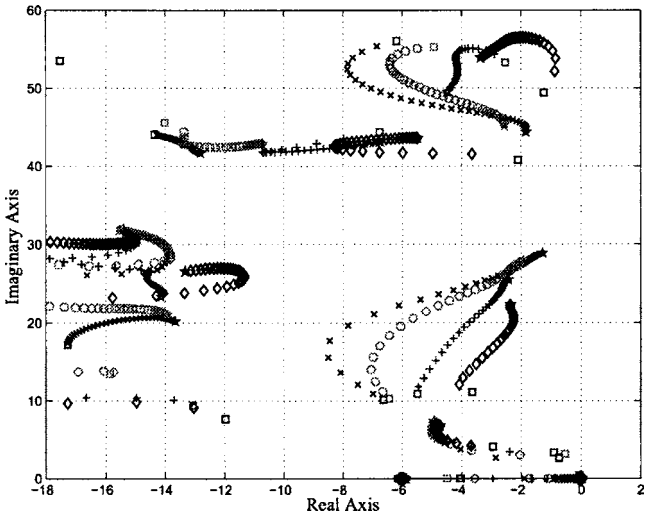

Fig. 14 Root-locus plots for: Straight running (×), 15 deg (∘), 30 deg (+), and 45 deg (◇) with speed the varied parameter from 7 m/s (□) to 75 m/s (⋆). The machine is fitted with the SC-3 network with the parameter values given in Table 1.

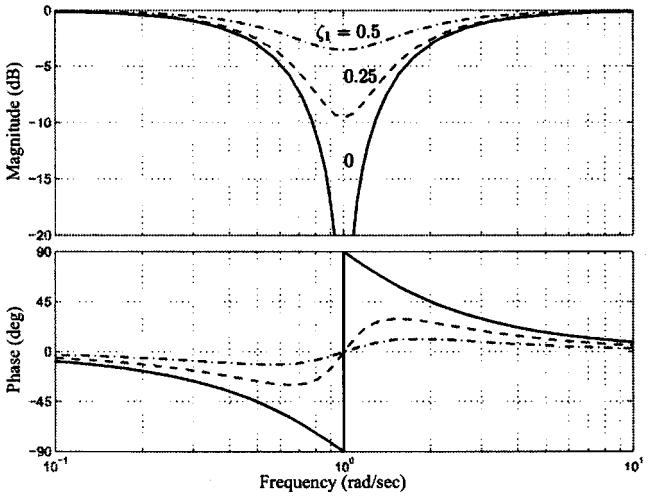

Fig. 15 Frequency responses for SC-4 with unity gain, resonant frequency ω_n=1, denominator damping ratio ζ_2=0.75 for three values of numerator damping ratio ζ_1

=0.1, ζ_2=0.4 and ω_n=25.

In the second phase of the design process, the unity-gain compensated Nyquist diagram is computed; the outcome is illustrated in Fig. 16. By studying the position of the $-1/K$ point as a function of K in Fig. 16, it can be seen that c_1=10 is a suitable damper value. As before, the other parameter values can be found by back substitution and are shown in Table 2.

As with the lead network illustrated above in Sec. 5.3, the notch compensator has good global properties which are demonstrated in Fig. 17. Again, good wobble- and weave-mode damping characteristics are evident.

5.5 Series Resonant Filter Design. The frequency-response characteristics of the SC-2 network are illustrated in Fig. 18. It is apparent from this figure that this network has the characteristics of an inerter at low frequencies and will introduce damping in the vicinity of ω_n, which should be tuned to the wobble-mode frequency. The damping ratio ζ is a free design parameter that can be chosen by trial and is used to provide the required phase compensation. As compared to the 90 deg of phase shift of SC-3, this network introduces 180 deg of phase and potentially has a fast phase transition in the vicinity of ω_n. These characteristics are useful in the present context. The correct value of the spring constant k can be derived from a compensated Nyquist plot in a manner analogous to the procedure explained in Secs. 5.3 and 5.4. Once k has been fixed, b can be found from ω_n and c from ζ; these details are left to the reader.

Table 2 Parameters for notch compensator (SC-4)

c_1	c_2	b	k
10	3.33	0.667	416.67

6 Optimization

The optimization of the mechanical networks in Fig. 11 will be studied from both a time- and a frequency-domain perspective. In order to do this, one has to deal with passivity constraints on the compensator parameters, the stability of the uncontrolled machine, as well as optimization across multiple linearized motorcycle models that "grid" the machine's operating envelope. The optimization studies will make use of the MATLAB sequential quadratic programing algorithm FMINCON [49], which accepts both linear and nonlinear equality and inequality constraints. In the case of the mechanical networks given in Fig. 11, passivity is ensured via the non-negativity of the network parameters. In the case of positive-real biquadratic functions, the constraints alluded to in Theorem 2 must be enforced.

6.1 Time Domain Criterion. The time-domain optimization of the networks in Fig. 11 seeks to maximize the motorcycle's lowest modal damping ratio for all the linearized models in the model set. In order to specify formally this optimization problem, it is helpful to refer to Fig. 19. In addition to the (hard) passivity constraints associated with the network parameter values, it is necessary to introduce stability constraints and a performance criterion for minimization. Recognizing that the low-frequency stability of the machine will be ensured by the rider, and not the compensation network, the stability constraint used here allows unstable low-frequency modes to remain in the right-half plane.

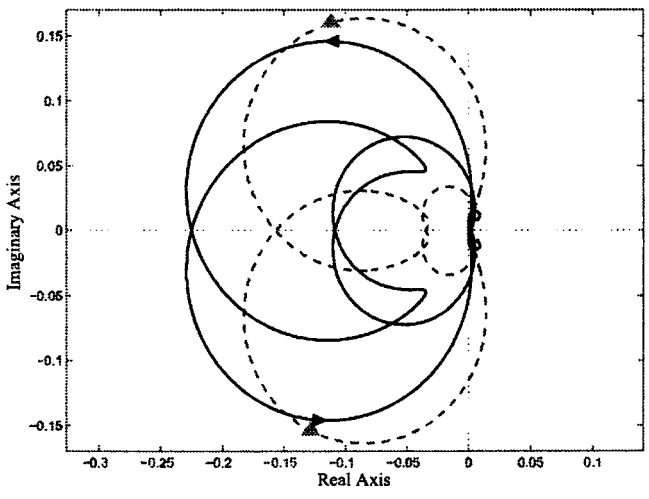

Fig. 16 Nyquist diagram for the straight-running open-loop motorcycle at a forward speed of 75 m/s. The solid line represents the nominal machine with a unity-gain steering damper and the dashed line the compensated system using the SC-4 network given in Fig. 11. The network parameters are c_1=1, ζ_1=0.1,ζ_2=0.4, and ω_n=25.

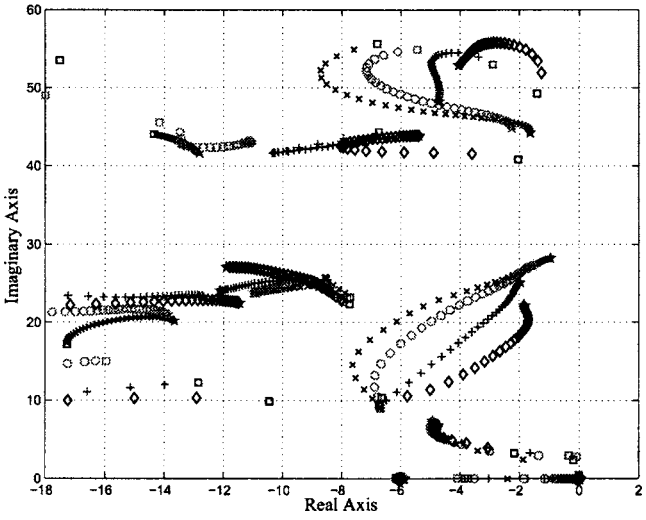

Fig. 17 Root-locus plots for: Straight running (×), 15 deg (∘), 30 deg (+), and 45 deg (◇) with speed the varied parameter for the compensated machine fitted with the network SC-4 with the parameters of Table 2. The speed is increased from 7 m/s (□) to 75 m/s (⋆).

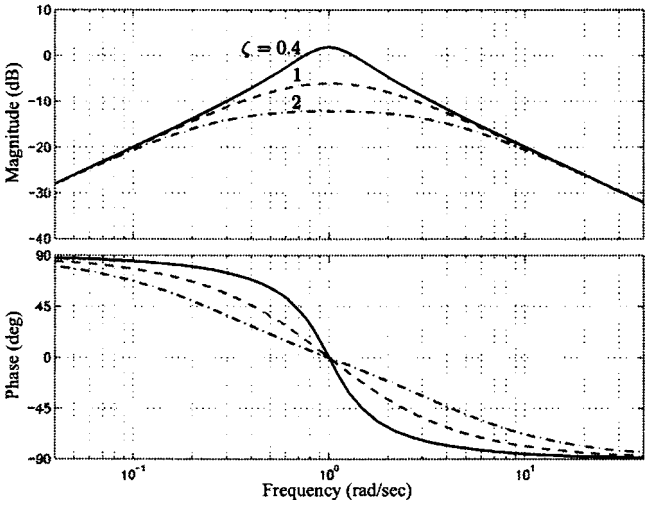

Fig. 18 Normalized frequency-response characteristics of the network SC-2 for three values of damping ratio

This is achieved via the requirement that only closed-loop eigenvalues with an imaginary part greater than j must be confined to the left-half of the complex plane. For illustration, this stability-related hard constraint is shown pictorially in Fig. 19(a) via the cross-hatching of the imaginary axis for values above j. As can be seen from Fig. 5 there is a low-frequency mode that is associated with rider upper-body oscillations. This mode is unstable for low speeds, and since it crosses the imaginary axis at $\sim 2.5j$, the optimization problem demands that the compensator stabilizes it. In contrast, no attempt is made to stabilize the marginally unstable capsize mode whose eigenvalue(s) is/are either real or has/have a very small imaginary part.

The set of linear motorcycle models used in solving the optimization problem grids the important part of the machine's operating conditions. This set is denoted Ω and contains linearized

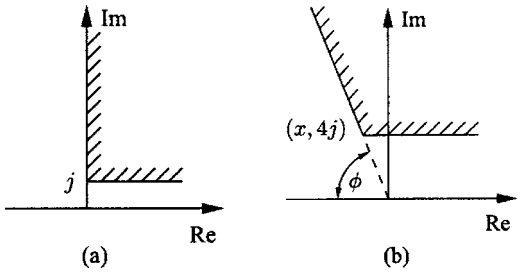

Fig. 19 (*a*) Stability constraint region and (*b*) damping ratio optimization region

models corresponding to trim roll angles of $0,3,6,\ldots,45$ deg and trim speeds of $7,9,11,\ldots,75$ m/s. The time-domain index for minimization is

$$J_t = \max_{\Omega} \max_{i} \{\tan(\phi_i)\} \tag{4}$$

in which the index i ranges over those modes with an imaginary part $>4j$. It is recognized that minimizing J_t will minimize ϕ_i for $0 \leq \phi_i \leq \pi/2$, and thus maximize the damping ratios, which are given by $\zeta_i = \cos(\phi_i)$. Geometrically, the optimizing algorithm will try to rotate the constant-damping-ratio line illustrated in Fig. 19(b) counterclockwise around the origin toward the negative real axis. The achieved minimum in J_t is associated with the least damped mode across the model set Ω.

6.2 Frequency-Domain Criterion. The optimization of linear systems via $\mathcal{H}_\infty$ frequency-response performance measures is a well-developed subject [45]. In the present context these measures are motivated by the role played by road displacement forcing in stability-related road traffic accidents [10]. The objective is to minimize the worst-case closed-loop gain from road forcing disturbances to steering angle (see Sec. 3 and Fig. 4) for all operating conditions, while simultaneously ensuring that the open-loop Nyquist diagram does not get "too close" to the -1 point. For each frequency ω_i, the

$$J_f = \max_{\Omega} \left\{ \max \left[\max_{\omega_i} \left| \frac{P_{11}(j\omega_i)}{1 - j\omega_i K(j\omega_i) P_{12}(j\omega_i)} \right|, \max_{\omega_i} \left| \frac{\gamma}{1 - j\omega_i K(j\omega_i) P_{12}(j\omega_i)} \right| \right] \right\} \tag{5}$$

distance between the Nyquist diagram and the -1 point is given by $|1 - j\omega_i K(j\omega_i) P_{12}(j\omega_i)|$. This is the modulus of the classical sensitivity function, which plays a central role in the subject of sensitivity and robustness of control systems [45]. In the work presented here, the multiobjective $\mathcal{H}_\infty$ index given in Eq. (5) will be used. The first term in (5) is the closed-loop transfer function between road forcing disturbances and the steering angle, while the second is a fixed constant times the inverse of the distance of closest approach between the Nyquist diagram and the -1 point. The positive reality constraints, the stability constraint, and the model set Ω used here are the same as those employed in the time-domain optimization problem described in Sec. 6.1. When evaluating J_f, a 100-point frequency list was used. These points were placed on a logarithmic scale that covered the range $\omega = 10^{1.3}$ to $\omega = 10^{1.85}$. This range was selected to include all the maxima in the index (5). The weighting factor on the second term was set by trial to $\gamma = 16$.

7 Optimization Results

Results pertaining to the performance of the optimized networks in Fig. 11, as well as the general positive real biquadratic function (SC-5) will now be given. The time-domain optimization results for the criterion described in Sec. 6.1 will be described first followed by the frequency-domain approach of Sec. 6.2. In appropriate cases, the optimization processes were initialized using the loop-shaping design methods described in Secs. 5.3–5.5.

7.1 Time-Domain Optimization. The results of optimizing each of the networks in Fig. 11 with the time-domain index (4) are given in Table 3. In addition to the optimal parameter values, the table also provides the minimum values achieved for the performance index (4), the trim condition at which the minimum was achieved, and the damped natural frequency of the least-damped mode at that trim state. The eigenvalues associated with this least-damped mode will lie against the damping ratio line in Fig. 19(b), while all the others will lie to the left of it. It can be seen from the

Table 3 Optimal Time-domain network parameter values

	Parameters	J_t	Maximum		
			(deg)	(m/s)	(rad/s)
SC-1	c=7.2526	112.99	45	11	54.56
SC-2	k=773.31	16.646	45	21	65.81
	c=22.723				
	b=0.32673				
SC-3	c=11.987	16.683	45	7	48.69
	k=416.54				
	b=0.32771				
SC-4	c_1=22.518	21.102	15	75	37.25
	c_2=0				
	k=101.74				
	b=0.6536				
SC-5	a_2=19.053	14.55	45	7	48.43
	a_1=180.29				
	a_0=11030.5				
	d_2=1.0				
	d_1=21.352				
	d_0=929.51				

table that the "best" network in this case is SC-2, and the least satisfactory is the conventional damper (SC-1). The performance of SC-2 (J_t=16.646) is only slightly worse than that of the general biquadratic positive real function SC-5 (J_t=14.55). Referring to Fig. 20, one observes the influence of the optimized SC-2 network on the compensated motorcycle's root-locus plot. As expected, the damping ratios of all the lightly damped motorcycle modes have been substantially increased with the wobble mode at ~66 rad/s against the constant damping ratio line. It can be shown that the networks SC-2, SC-3, and SC-4 substantially increase the highest achievable stable straight-running speed for the motorcycle modeled here ([48], Table 4).

Figure 21 shows the variation of J_t with operating point in the case of the optimal damper SC-1. The figure reflects the fact that there is a compromise between high-speed-weave and low-speed-wobble operating conditions with conventional dampers. In particular, at a speed of 11 m/s and a roll angle of 45 deg, the wobble damping ratio is only ζ=0.009. For high-speed straight-running, the weave mode is similarly lightly damped. A J_t performance surface for SC-2 is given in Fig. 22. It is clear from this figure that although the machine retains its tendency to have a lightly damped weave mode under high-speed straight-running conditions, and a lightly damped wobble mode under lower-speed high-roll-angle conditions, the worst case damping ratio has increased significantly to ζ=0.06. The general biquadratic positive real compensator increases this value only slightly to ζ=0.069.

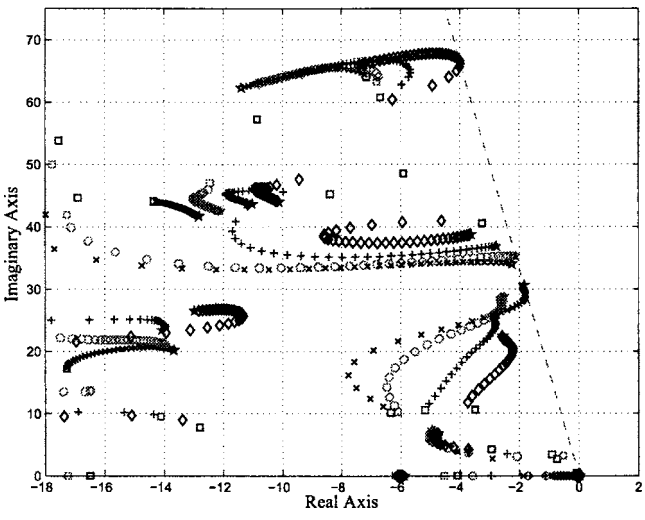

Fig. 20 Root-locus plots for: Straight running (×), 15 deg (∘), 30 deg (+), and 45 deg (◇) of roll angle with speed the varied parameter. The network SC-2 is fitted and was optimized to minimize the performance index (4). The speed is increased from 7 m/s (□) to 75 m/s (⋆).

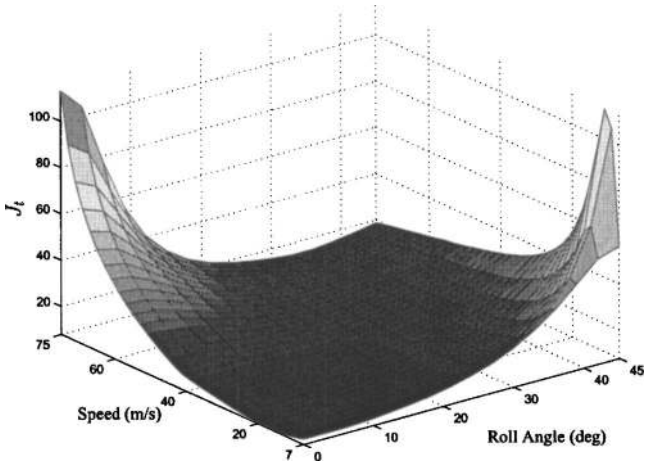

Fig. 21 Cost function J_t for 7–75 m/s and 0–45 deg lean with the motorcycle fitted with the optimized SC-1 compensated system

Before leaving the time-domain results, it is interesting to consider the sensitivity of the designs obtained. Figure 23 shows the Nyquist diagrams associated with the nominal damper and the series resonant network SC-2. It is clear that in the latter case the optimized network offers poor gain and phase margins; indeed these were not included in the optimization problem formulation. This suggests the possibility that parameter variations and/or modeling inaccuracies may result in the instability of the weave mode.

Figure 24 shows the sensitivity of the wobble mode at 11 m/s and 45 deg to variations in the nominal steering damper parameter value, and the parameter values of each of the networks SC-2 to SC-4 inclusive. As compared to the other networks, the SC-2 network wobble-mode damping performance appears especially sensitive to variations in each of its three parameters. This is particularly true in the case of the spring constant and the inertance value, which together dictate the network's resonant frequency;

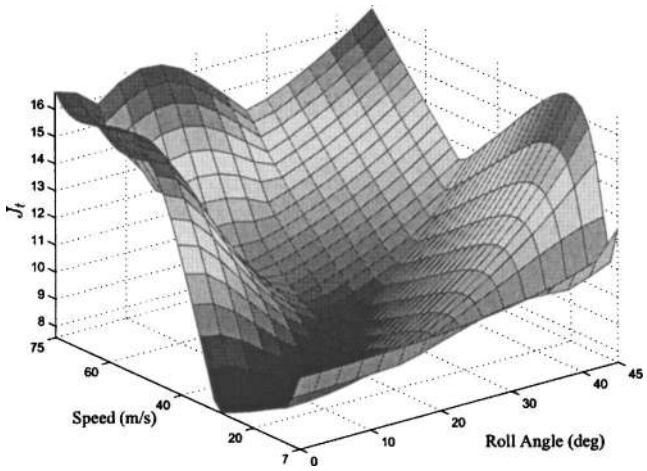

Fig. 22 Cost function J_t for 7–75 m/s and 0–45 deg lean with the motorcycle fitted with the optimized SC-2 compensated system

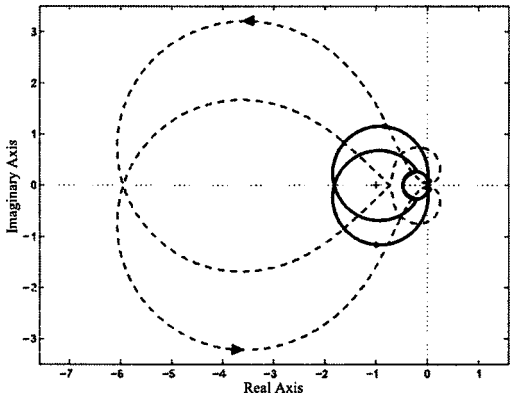

Fig. 23 Nyquist diagrams for the open-loop motorcycle with a forward speed of 75 m/s and a roll angle of 15 deg. The solid line represents the machine fitted with the nominal steering damper, and the dashed line represents the machine fitted with the time-domain optimized SC-2 network.

see (2). A similar calculation of sensitivities will also be done in the next section where the cost criterion (5) specifically includes a robustness enhancing term.

7.2 Frequency-Domain Optimization. The results of optimizing each of the networks in Fig. 11 with the frequency-domain index (5) are given in Table 4. In addition to the optimal parameter values the table also provides the minimum values achieved for the performance index (5), the trim condition at which the minimum was achieved, and the frequencies corresponding to the frequency-response peaks associated with the limiting value of J_f. It is evident from the table that the "best" network in this case is again SC-2 and the least satisfactory is the conventional steering damper SC-1. As one would now expect, a marginally better performance is achieved by the general biquadratic positive real compensator SC-5. It is also clear that in each case the wobble mode is dictating the lowest achievable value of J_f. In the case of SC-2, J_f=40.576 was obtained, and so the closest distance of approach between the Nyquist plot and the -1 point is $\geqslant 16/40.576$ $=0.394$; recall that $\gamma=16$ was used in (5). As a result, improved gain and phase margins have been achieved as compared with the time-domain optimized SC-2 network.

Table 4 Optimal frequency-domain network parameter values

	Parameters	J_f	Maximum		
			(deg)	(m/s)	(rad/s)
SC-1	c=8.0695	109.8412	45	9	52.97
SC-2	k=594.08	40.576	45	7	49.95
	c=13.716				
	b=0.24252				
SC-3	c=8.0941	49.05	45	7	49.21
	k=281.2483				
	b=0.2387				
SC-4	c_1=13.322	46.155	45	7	48.89
	c_2=0.00070281				
	k=256.66				
	b=0.71191				
SC-5	a_2=13.944	37.5896	45	7	49.16
	a_1=85.172				
	a_0=11167				
	d_2=1.0				
	d_1=13.535				
	d_0=941.83				

Figure 25 shows the locus of the motorcycle's important modes for a wide range of speeds and roll angles in the case that the optimized SC-2 network is fitted. As with the time-domain optimized parameters, this network achieves improved damping ratios for each of the machine's lightly damped modes. Figure 26 shows the road-forcing response

$$\max_{\omega_i} \left| \frac{P_{11}(j\omega_i)}{1 - j\omega_i K(j\omega_i) P_{12}(j\omega_i)} \right|$$

as the trim state ranges over the motorcycle's cornering regime; under straight-running conditions, the road-forcing response goes to zero. In common with each of the other networks, the highest gain values occur at low speeds and high roll angles, and correspond to the excitation of the wobble mode. As one would expect, relatively high values of road forcing gain are also achieved under high-speed low-roll-angle conditions (see 75 m/s and 15 deg roll

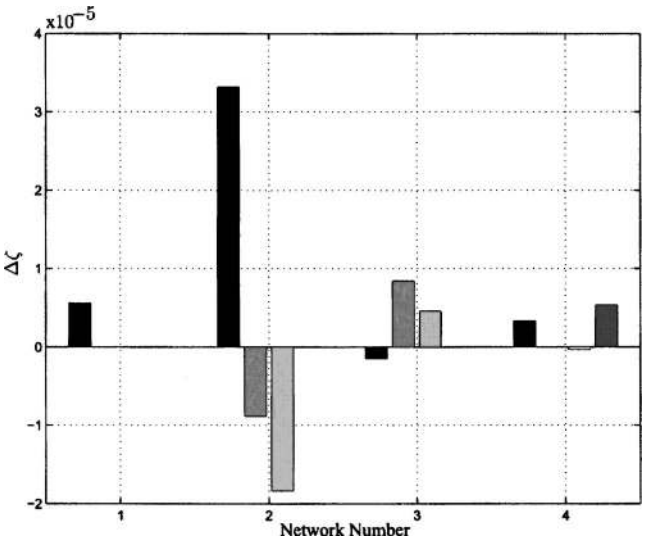

Fig. 24 The vertical axis shows changes in the damping ratio of the wobble mode for single-parameter variations in each of the time-domain optimized networks: nominal steering damper SC-1 to SC-4. The trim condition is 45 deg and 11 m/s; the parameter values are adjusted by 0.01%. The order of the parameters in each group is the same as that given in Table 3.

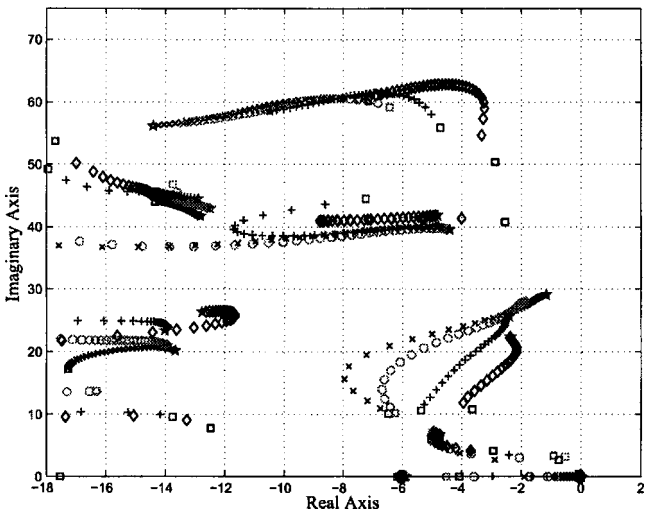

Fig. 25 Root-locus plots for: Straight running (×), 15 deg (∘), 30 deg (+), and 45 deg (◇) of roll angle, with the speed varied from 7 m/s (□) to 75 m/s (⋆). The network SC-2 is fitted with its parameters set to minimize J_f in (5).

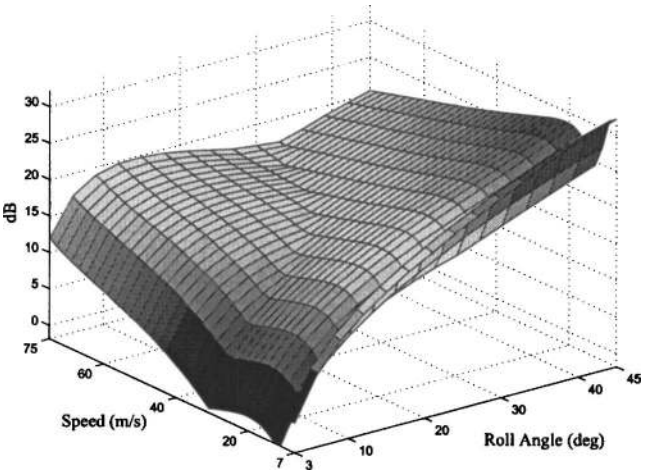

Fig. 26 Road forcing gain for 7–75 m/s and 3–45 deg roll angle for the frequency-domain optimized SC-2 compensated system

angle); this is a feature shared by each of the other networks. The road forcing characteristics of the machine are also illustrated by the frequency-response plots shown in Figs. 27 and 28. As is evident from the first of these figures, the SC-2 network decreases the peak wobble-mode road-forcing gain by ~15 dB. The trim condition selected corresponds to an equilibrium state in which the wobble mode is particularly vulnerable to road displacement forcing. The second of these figures corresponds to a high-speed trim condition in which the weave mode is particularly vulnerable to road displacement forcing. In this case the SC-2 network is seen to reduce the weave-mode peak by ~3 dB as compared to the nominal damper that is fitted to the production machine.

In order to further investigate the robustness of the frequency-domain optimized networks, a study was carried out that investigates the range over which the network parameters can be varied, one at a time, without destabilizing the machine. Table 5 shows the effect of changing individual network parameters. As expected, in the case of the damper, the wobble mode will be destabilized if the damper value is too low, while the weave mode is

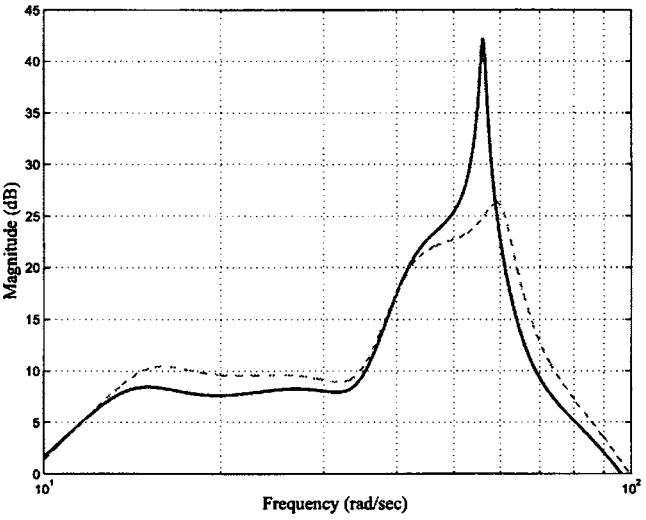

Fig. 27 Bode magnitude plot for road displacement forcing (0 dB=1 rad/m). The machine is operating at a forward speed of 15 m/s and a roll angle of 45 deg. The solid line represents the nominal machine, and the dashed line the machine fitted with the frequency-domain optimized SC-2 network.

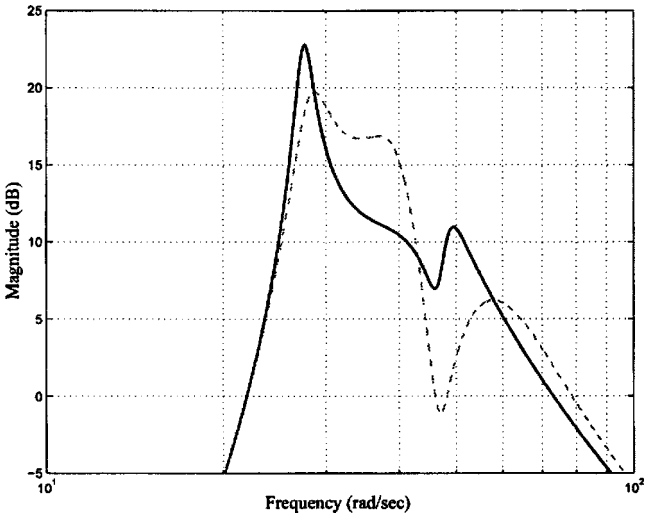

Fig. 28 Bode magnitude plot for road displacement forcing (0 dB=1 rad/m). The machine is operating at a forward speed of 75 m/s and a roll angle of 15 deg. The solid line represents the nominal machine, and the dashed line the machine fitted with the frequency-domain optimized SC-2 network.

destabilized if it is too large. In comparison to the other networks, the stable range of the SC-1 damper values is relatively small. Without exception, in the case of the other networks, the various parameter values can be varied over a much larger range without instability.

Figure 29 shows that the frequency-domain optimized SC-2 network has improved wobble-mode sensitivity properties as compared to its time-domain counterpart (Fig. 24). With that said, compared to the other networks, the need to "tune" this network to the low-speed high-roll-angle, wobble-mode frequency renders it relatively sensitive to parameter variations under these conditions. This relatively high low-speed high-roll-angle sensitivity characteristic has to be set against its excellent overall nominal performance.

We conclude with a brief examination of the motorcycle's sensitivity to machine parameter variations. Intuitively, one would expect any difficulty to be most apparent in the parameters which specify the dynamics of the steering system and the "front-end" of the motorcycle. These include geometry-related parameters, the front-frame stiffness and the steering system inertia parameters. The sensitivities to variations in a selection of these parameters is given in Fig. 30. It is apparent from this diagram that the damping ratio sensitivity of the wobble mode, at the indicated trim condition, for the network SC-2, is particularly large in respect of the front wheel attachment point, the x-axis component of the twist axis joint with the main frame, the front tire crown radius, and the steering head angle. The wobble-mode damping ratio sensitivities to the front frame stiffness, and the mass and moment of inertia parameters are comparatively low. It is important to note from Fig. 30 that the frequency-domain optimized networks have sensitivities that are comparable with those of the conventional damper. This indicates that the robustness of these networks will be no worse than that of the conventional damper.

8 Conclusions

This paper has introduced the idea of replacing a conventional steering damper with a mechanical network comprising spring(s), damper(s), and inerter(s) [30] on a high-performance motorcycle. The study has used an advanced motorcycle simulation model [5,8,9] to demonstrate that this can lead to clear performance benefits in the wobble- and weave-mode damping. Methods of passive electrical circuit synthesis [33,34] that have been recast into a

Table 5 Stable ranges for single parameter variations. The frequency of oscillation at instability and the associated trim states are also noted. The frequency-domain optimized network parameters are used. The operating conditions considered include forward speeds from 7 to 75 m/s and roll angles from 0 to 45 deg.

Network	Parameters	Stable range	Lower instability	Upper instability
SC-1	$c=8.0695$	$6.1328 \leqslant c \leqslant 9.1992$	(45 deg,11 m/s) 54.4036 rad/s	(0 deg,75 m/s) 28.3597 rad/s
SC-2	$k=594.08$	$433.6784 \leqslant k \leqslant 1969.4$	(45 deg,15 m/s) 60.0887 rad/s	(0 deg,73 m/s) 42.3941 rad/s
	$c=13.716$	$6.3779 \leqslant c \leqslant 27.0205$	(45 deg,11 m/s) 54.7304 rad/s	(0 deg,75 m/s)36.5001 rad/s
	$b=0.24252$	$0.1601 \leqslant b \leqslant 0.3771$	(0 deg,73 m/s) 42.4039 rad/s	(0 deg,75 m/s) 29.3787 rad/s
SC-3	$c=8.0941$	$4.4518 \leqslant c \leqslant 13.0315$	(0 deg,75 m/s) 31.1644 rad/s	(0 deg,73 m/s) 41.2790 rad/s
	$k=281.2483$	$32.3436 \leqslant k \leqslant 442.9661$	(0 deg,69 m/s) 45.1722 rad/s	(0 deg,75 m/s)37.4435 rad/s
	$b=0.2387$	$0.1719 \leqslant b \leqslant 0.3103$	(0 deg,73 m/s) 42.4861 rad/s	(0 deg,75 m/s) 30.2920 rad/s
SC-4	$c_1=13.322$	$5.9949 \leqslant c_1 \leqslant 26.644$	(45 deg,11 m/s) 53.9057 rad/s	(0 deg,75 m/s) 36.7354 rad/s
	$c_2=0.00070281$	$0 \leqslant c_2 \leqslant 29.5$		(0 deg,75 m/s) 28.5082 rad/s
	$k=256.66$	$0 \leqslant k \leqslant 730.1977$		(0 deg,75 m/s) 42.396 rad/s
	$b=0.71191$	$0.4485 \leqslant b \leqslant 1.1569$	(0 deg,73 m/s) 42.5535 rad/s	(0 deg,75 m/s) 29.3067 rad/s

mechanical engineering setting via the introduction of the inerter play a central role in this research. Classical frequency-response methodologies [47] also play an important role. A number of steering compensators are optimized and analyzed in the spirit of classical time-domain and $\mathcal{H}_\infty$ control systems design ideas [45].

The investigation in this paper was prompted by the often reported poor performance of high-powered sports motorcycles operating at high speed. The results of Sec. 4 show that the nominal machine is vulnerable to high-speed weave, particularly under straight-running or low-roll-angle conditions, and low-speed wobble, particularly at high roll angles. This initial study shows why there is only a small usable range of steering damper parameter values and illustrates why conventional motorcycles are dogged by an apparently intractable wobble-weave-mode damping compromise.

The results in Sec. 5.1 show that a steering damper is an effective means of damping the wobble mode, but that it has a deleterious effect on the weave mode. These results also show that a steering inerter can improve the damping of the weave mode. Taken in combination, these observations motivated the study of the simple mechanical networks presented in Fig. 11. In each case the network parameters can be selected so that they "look like" a damper above the weave-mode frequency band, while adopting the mantle of an inerter at lower frequencies. Three network configurations with these general characteristics were analyzed in detail. The network SC-2 introduces low-frequency inertance and narrowband wobble-mode damping, SC-3 is in essence a mechanical lead compensator [47], while the notch filter characteristics of SC-4 are used to shield the weave mode from the negative effect of a steering damper. Simple frequency-response design procedures are presented for each of these networks. In a first design step, each compensation network's natural frequency and damping ratio(s) are chosen. In a second step, which is conducted after the unity-gain compensated Nyquist diagram is plotted, the network's spring constant (SC-2), or (one of) the network's damper values is selected (SC-3 and SC-4). The remaining parameters are found by back substitution. It is demonstrated that these hand-designed networks have greatly improved performance characteristics as compared to the nominal machine.

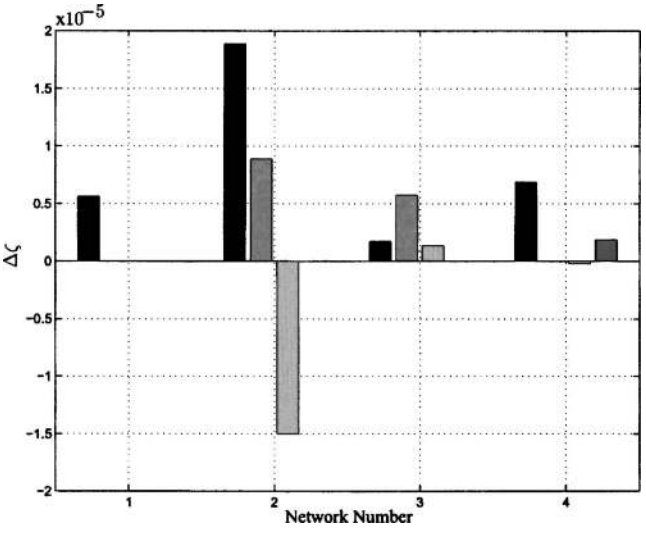

Fig. 29 Compensator parameter sensitivities for the wobble mode at 45 deg and 11 m/s. The vertical axis shows the change in the damping ratio for a 0.01% change in each parameter. The frequency-domain optimized networks are used; the first network is the nominal steering damper. The parameters in each of the four network groups (SC-1 to SC-4) adopt the ordering in Table 4.

Time- and frequency-domain design optimization frameworks are described in Sec. 6, which accommodate passivity and robust stability. The philosophy behind these frameworks comes from traditional second-order system ideas [47] and robust control theory [45]. The parameter optimization is achieved via a sequential quadratic programing algorithm [49]. Given the nonlinear characteristics of motorcycles, as they range over their operating envelope, it is vital that the steering compensator networks are optimized across the machine's entire working regime. This was achieved using a set of linearized models that grid the motorcycle's operating domain.

The results presented in Sec. 7 show that substantial global performance improvements, as compared to conventional steering dampers, are achievable using the various network configurations given in Fig. 11. In the case of both time- and frequency-domain optimization criteria, the nominal performance of the network SC-2 is excellent and only slightly worse than that of the ideal biquadratic positive real compensator SC-5. Important facets of this improved performance come in the form of substantially improved wobble- and weave-mode damping, as well as improvements in the motorcycle's straight-running top-speed stability. Sensitivity studies, and gain and phase margin considerations, indicated that parameter optimization exercises should be "robustified" against modeling uncertainties and parameter drift. In the case of the frequency-domain criterion J_f, given in Eq. (5), an explicit robust stability property is introduced. The operating conditions associated with worst-case wobble- and weave-mode damping are identified, and the road disturbance rejection properties of the various steering compensators are studied and greatly improved there. Worst-case wobble performance occurs under low-speed high-roll-angle conditions, while worst-case weave performance occurs when the machine is operating under high-speed low-roll-angle circumstances. As expected, each of the steering compensators is particularly effective against wobble. Impor-

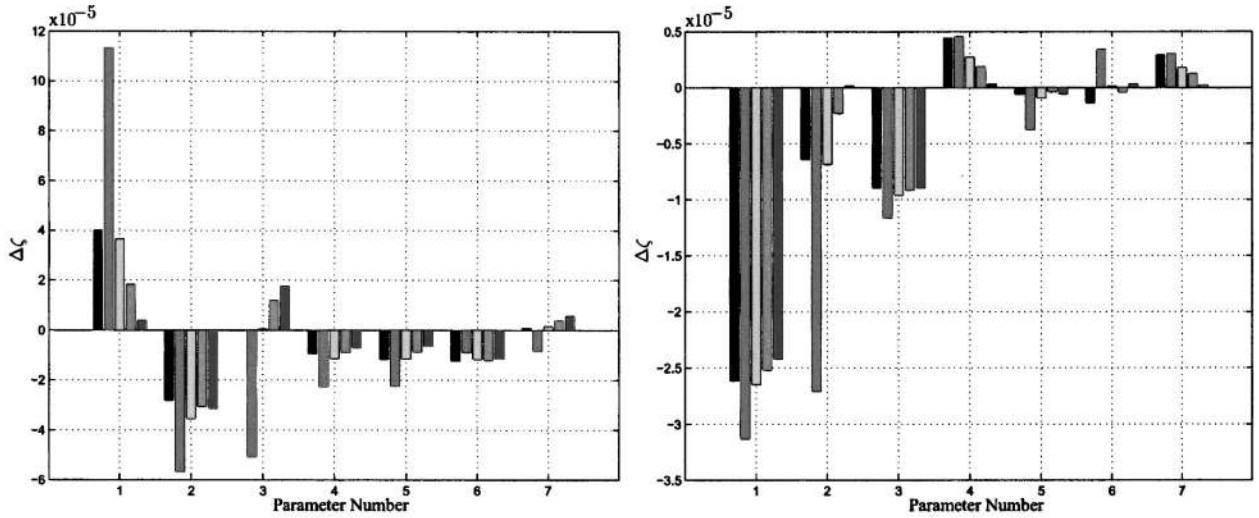

Par. Number	Symbol	Name
1	x6	x co. of front wheel attachment point
2	z6	z co. of front wheel attachment point
3	x2	x co. of twist axis joint with main frame
4	x5	x co. of center of mass of front susp. body
5	x3	x co. of center of mass of front steer body
6	x8	x co. of center of mass of the main frame
7	z2	z co. of twist axis joint with main frame

Par. Number	Symbol	Name
1	f_tcrad	Front tire crown radius
2	head_ang	Head angle
3	Mmain	Main body mass
4	Iff_strz	Front frame steering inertia
5	Kp_twst	Twist flexibility stiffness
6	Imnz	Main body yaw inertia
7	Ifwx	Front wheel x moment of inertia

Fig. 30 Wobble-mode damping ratio sensitivities at 45 deg and 11 m/s. The vertical axis shows the change in the damping ratio for a 0.01% change in each of the parameters shown in the tables below the subfigures. The bars are shown in groups of five; each group represents the steering-compensated vehicle with the frequency-domain optimized networks in the order: nominal steering damper, SC-2, SC-3, SC-4, and SC-5.

tantly, enhanced weave-mode performance can be achieved simultaneously. In each case, the network performance is more sensitive to front-end parameter variations than to those that do not directly affect the machine's steering behavior.

The general issue of the practical implementation of passive mechanical compensators is the subject of ongoing investigation. A prototype for the SC-2 network has been built and tested at the Cambridge University Engineering Department comprising an epicyclic gear mechanism. For steering compensators to be deployed on production motorcycles, issues such as the selection of optimal gear ratios for the inerters, correct dimensioning of the device in order that it is robust enough to withstand the wear and tear of normal usage, and packaging will be important to consider.

It has not escaped our notice that the use of active steering compensation is a potentially attractive possibility by, for example, making use of a steering torque motor, a digital signal processing chip set, and a speed- and steer-angle sensing arrangement. In this case, the correct dimensioning of the torque motor and its associated gearing and power electronics is likely to be of central importance. This approach has several potential advantages: one is no longer restricted to positive-real compensators, it is no longer necessary for the device to be low-order, and finally, adaptive systems are a practical possibility. This topic is the subject of ongoing research.

Appendix

Proof of Theorem 2. Suppose that $Z(s)$ is positive real. By calculation

$$Z(j\omega) = \frac{(a_0 - a_2\omega^2) + j\omega a_1}{(d_0 - d_2\omega^2) + j\omega d_1} = \frac{a_2 d_2 \omega^4 + \omega^2(a_1 d_1 - a_0 d_2 - a_2 d_0) + a_0 d_0}{(d_0 - d_2\omega^2)^2 + \omega^2 d_1^2} + \text{Im} \quad \text{(A1)}$$

in which Im is the imaginary part of $Z(j\omega)$. Since the real part of $Z(j\omega)$ is non-negative, after setting $x=\omega^2$, we obtain

$$f(x) = a_2 d_2 x^2 + (a_1 d_1 - a_0 d_2 - a_2 d_0)x + a_0 d_0 \geq 0$$

for all $x \geq 0$. In the case that $a_2 d_0 + a_0 d_2 - a_1 d_1 \geq 0$, it follows from the properties of quadratic equations that $f(x) \geq 0$ implies

$$4a_2 a_0 d_2 d_0 \geq (a_1 d_1 - a_0 d_2 - a_2 d_0)^2$$

$$\Leftrightarrow 2\sqrt{a_0 d_2}\sqrt{a_2 d_0} \geq a_0 d_2 + a_2 d_0 - a_1 d_1$$

$$\Leftrightarrow a_1 d_1 \geq (\sqrt{a_0 d_2} - \sqrt{a_2 d_0})^2 \quad \text{(A2)}$$

which shows that the inequality in the theorem is necessary. In the case that $a_0 d_2 + a_2 d_0 - a_1 d_1 \leq 0$, we observe that the inequality is again necessary.

Let us now turn to the sufficiency of the inequality in the theorem. Since d_0, d_1 and d_2 are all nonnegative, $Z(s)$ has no poles in the open right-half plane. If the inequality is satisfied, it follows that (A2) holds, which implies that $f(x) \geq 0$ for all x. Hence, $\text{Re}[Z(j\omega)] \geq 0$ for all $j\omega$ values that are not poles of $Z(s)$. To complete the proof we need to check the residue condition for all cases in which $Z(s)$ has poles on the imaginary axis, or infinity.

Case 1. Poles at the origin. This situation occurs when $d_2 \geqslant 0$, $d_1 \geqslant 0$ and $d_0 = 0$, in which case

$$Z_0 = \lim_{s \to 0} \frac{s(a_2 s^2 + a_1 s + a_0)}{s(d_2 s + d_1)} = \frac{a_0}{d_1}$$

when $d_1 > 0$. If $d_1 = 0$ and $d_2 > 0$, the inequality in the theorem $\Rightarrow a_0 = 0$ and $Z_0 = a_1/d_2$. In each case $Z_0 \geqslant 0$.

Case 2. Poles at infinity. This occurs when $d_2 = 0$, $d_1 \geqslant 0$ and $d_0 \geqslant 0$, in which case

$$Z_\infty = \lim_{s \to \infty} \frac{a_2 s^2 + a_1 s + a_0}{s(d_1 s + d_0)} = \frac{a_2}{d_1}$$

when $d_1 > 0$. If $d_1 = 0$, the inequality in the theorem $\Rightarrow a_2 = 0$ and $Z_\infty = a_1/d_0$. In each case, $Z_\infty \geqslant 0$.

Case 3. Poles on the imaginary axis with finite positive modulus. This occurs when $d_2 > 0$, $d_1 = 0$ and $d_0 > 0$, in which case

$$Z_{j\omega_0} = \lim_{s \to j\omega_0 = j\sqrt{d_0/d_2}} (s - j\omega_0) \frac{a_2 s^2 + a_1 s + a_0}{d_2 s^2 + d_0}$$

$$= \frac{a_0 d_2 - a_2 d_0 + j\sqrt{d_2 d_0}\, a_1}{2jd_2\sqrt{d_0 d_2}}.$$

Since $d_1 = 0$, it follows from the inequality in the theorem that $a_0 d_2 = a_2 d_0$ and so $Z_{j\omega_0} = a_1/2d_2 \geqslant 0$. A similar calculation also shows that $Z_{-j\omega_0} = a_1/2d_2 \geqslant 0$.

References

[1] Sharp, R. S., 1971, "The Stability and Control of Motorcycles," J. Mech. Eng. Sci., **13**(5), pp. 316–329.

[2] Sharp, R. S., 1994, "Vibrational Modes of Motorcycles and Their Design Parameter Sensitivities," *Vehicle NVH and Refinement, Proc Int Conf.* Mech. Eng. Publications, London, May 3–5, pp. 107–121.

[3] Limebeer, D. J. N., Sharp, R. S., and Evangelou, S., 2001, "The stability of motorcycles under acceleration and braking," Proc. Inst. Mech. Eng., Part C: J. Mech. Eng. Sci., **215**(9), pp. 1095–1109.

[4] Koenen, C., 1983, "The Dynamic Behaviour of Motorcycles When Running Straight Ahead and When Cornering," Ph.D. dissertation, Delft University of Technology.

[5] Sharp, R. S., and Limebeer, D. J. N., 2001, "A Motorcycle Model for Stability and Control Analysis," Multibody Syst. Dyn., **6**(2), pp. 123–142.

[6] Cossalter, V., and Lot, R., 2002, "A Motorcycle Multi-Body Model for Real Time Simulations Based on the Natural Coordinates Approach," Veh. Syst. Dyn., **37**(6), pp. 423–447.

[7] Sharp, R. S., 2001, "Stability, Control and Steering Responses of Motorcycles," Veh. Syst. Dyn., **35**(4–5), pp. 291–318.

[8] Sharp, R. S., Evangelou, S., and Limebeer, D. J. N., 2003, "Improved Modelling of Motorcycle Dynamics," *ECCOMAS Thematic Conference on Advances in Computational Multibody Dynamics*, J. Ambrósio, ed., Lisbon, July 1–4, Paper No. MB2003-029 (CD-ROM).

[9] Sharp, R. S., Evangelou, S., and Limebeer, D. J. N., 2004, "Advances in the Modelling of Motorcycle Dynamics," Multibody Syst. Dyn., **12**(3), pp. 251–281.

[10] Limebeer, D. J. N., Sharp, R. S., and Evangelou, S., 2002, "Motorcycle Steering Oscillations Due to Road Profiling," ASME J. Appl. Mech., **69**(6), pp. 724–739.

[11] Döhring, E., 1956, "Steering Wobble in Single-Track Vehicles," ATZ, **58**(10), pp. 282–286.

[12] Eaton, D. J., 1973, "Man-Machine Dynamics in the Stabilization of Single-Track Vehicles," Ph.D. dissertation, University of Michigan.

[13] Watanabe, Y., and Yoshida, K., 1973, "Motorcycle Handling Performance for Obstacle Avoidance," *2nd Int. Congress on Automotive Safety*, San Francisco.

[14] Jennings, G., 1974, "A Study of Motorcycle Suspension Damping Characteristics," SAE Paper No. 740628.

[15] Roe, G. E., and Thorpe, T. E., 1976, "A Solution of the Low-Speed Wheel Flutter Instability in Motorcycles," J. Mech. Eng. Sci., **18**(2), pp. 57–65.

[16] Verma, M. K., 1978, "Theoretical and Experimental Investigation of Motorcycle Dynamics," Ph.D. dissertation, University of Michigan.

[17] McKibben, J. S., 1978, "Motorcycle Dynamics – Fact, Fiction and Folklore," SAE Paper No. 780309.

[18] Aoki, A., 1979, "Experimental Study on Motorcycle Steering Performance," SAE Paper No. 790265.

[19] Weir, D. H., and Zellner, J. W., 1979, "Experimental Investigation of the Transient Behaviour of Motorcycles," SAE Paper No. 790266.

[20] Thomson, B., and Rathgeber, H., 1984, "Automated Systems Used for Rapid and Flexible Generation of System Models Exemplified by a Verified Passenger Car and a Motorcycle Model," *Dynamics of Vehicles on Roads and on Railway Tracks*, J. K. Hedrick, ed., Swets and Zeitlinger, Lisse, pp. 645–654.

[21] Bayer, B., 1988, "Flattern und Pendeln bei Krafträdern," Auto. Indust., **2**, pp. 193–197.

[22] Takahashi, T., Yamada, T., and Nakamura, T., 1984, "Experimental and Theoretical Study of the Influence of Tires on Straight-Running Motorcycle Weave Response," Paper No. SAE 840248.

[23] Otto, W. M., 1980, "Effect of Motorcycle Accessories on Stability," *Proc. International Motorcycle Safety Conference*, Linthicum, MD May, Motorcycle Safety Foundation, Washington, DC, pp. 1560–1581.

[24] Sugizaki, M., and Hasegawa, A., 1988, "Experimental Analysis of Transient Response of Motorcycle Rider Systems," SAE 881783.

[25] Biral, F., Bortoluzzi, D., Cossalter, V., and Da Lio, M., 2003, "Experimental Study of Motorcycle Transfer Functions for Evaluating Handling," Veh. Syst. Dyn., **39**(1), pp. 1–26.

[26] Foale, T., (2002), "Motorcycle Handling and Chassis Design—The Art and Science," available at http://www.tonyfoale.com

[27] Sharp, R. S., and Alstead, C. J., 1980, "The Influence of Structural Flexibilities on the Straight Running Stability of Motorcycles," Veh. Syst. Dyn., **9**(6), pp. 327–357.

[28] Spierings, P. T. J., 1981, "The Effects of Lateral Front Fork Flexibility on the Vibrational Modes of Straight-Running Single-Track Vehicles," Veh. Syst. Dyn., **10**(1), pp. 21–35.

[29] Wakabayashi, T., and Sakai, K., 2004, "Development of Electronically Controlled Hydraulic Rotary Steering Damper for Motorcycles," *International Motorcycle Safety Conference*, IFZ, Munich, pp. 1–22.

[30] Smith, M. C., 2002, "Synthesis of Mechanical Networks: The Inerter," IEEE Trans. Autom. Control, **47**(10), pp. 1648–1662.

[31] Smith, M. C., 2001, "Force-Controlling Mechanical Device," patent pending, International Application No. PCT/GB02/03056, July 4.

[32] Shearer, J. L., Murphy, A. T., and Richardson, H. H., 1967, *Introduction to System Dynamics*, Addison-Wesley, Reading, MA.

[33] Anderson, B. D. O., and Vongpanitlerd, S., 1973, *Network Analysis and Synthesis*, Prentice-Hall, Englewood Cliffs, NJ.

[34] Newcomb, R. W., 1966, *Linear Multiport Synthesis*, McGraw-Hill, New York.

[35] Valkenburg, M. E. V., 1960, *Introduction to Modern Network Synthesis*, Wiley, New York.

[36] Foster, R. M., and Ladenheim, E. L., 1963, "A Class of Biquadratic Impedances," IEEE Trans. Circuit Theory, **10**, pp. 262–265.

[37] Smith, M. C., and Wang, F.-C., 2004, "Performance Benefits in Passive Vehicle Suspensions Employing Inerters," Veh. Syst. Dyn., **42**(4), pp. 235–257.

[38] de Vries, E. J. H., and Pacejka, H. B., 1998, "The Effect of Tyre Modeling on the Stability Analysis of a Motorcycle," *Proc. AVEC'98*, SAE of Japan, Nagoya, pp. 355–360.

[39] de Vries, E., and Pacejka, H., 1998, "Motorcycle Tyre Measurements and Models," Proc. 15th IAVSD Symposium on the Dynamics of Vehicles on Roads and on Tracks, L. Palkovics, ed., Budapest, August 25–29 1997, Veh. Syst. Dyn., **28**(Suppl.), pp. 280–298.

[40] Pacejka, H. B., 2002, *Tyre and Vehicle Dynamics*, Butterworth Heinemann, Oxford.

[41] Tezuka, Y., Ishii, H., and Kiyota, S., 2001, "Application of the Magic Formula Tire Model to Motorcycle Maneuverability Analysis," JSAE Rev., **22**, pp. 305–310.

[42] Cossalter, V., Doria, A., Lot, R., Ruffo, N., and Salvador, M., 2003, "Dynamic Properties of Motorcycle and Scooter Tires: Measurement and Comparison," Veh. Syst. Dyn., **39**(5), pp. 329–352.

[43] Evangelou, S., 2004, "The Control and Stability Analysis of Two-Wheeled Road Vehicles," Ph.D. thesis, Imperial College, London.

[44] Anon, , 1998, *Autosim* 2.5+ *Reference Manual*, Mechanical Simulation Corp., Ann Arbor, http://www.carsim.com

[45] Green, M., and Limebeer, D. J. N., 1995, *Linear Robust Control*, Prentice-Hall, Englewood Cliffs, NJ.

[46] Papageorgiou, C., and Smith, M. C., 2004, "Positive Real Synthesis Using Matrix Inequalities for Mechanical Networks: Application to Vehicle Suspension," *43rd IEEE Conference on Decision and Control*, Dec. 14–17.

[47] Dorf, R. C., and Bishop, R. H., 2001, *Modern Control Systems*, Prentice-Hall, Englewood Cliffs, NJ.

[48] Evangelou, S., Limebeer, D. J. N., Sharp, R. S., and Smith, M. C., 2005, "Mechanical Steering Compensators for High-Performance Motorcycles," Cambridge Engineering Department, Tech. Report No. CUED/F-INFENG/TR 535.

[49] The Mathworks Inc., 2000, *MATLAB 6 Reference Manual* http://www.mathworks.com